Preprint ANL/MCS-P1753-0510

Mathematics and Computers in Simulation 00 (2010) 1–26

An O(m+n) measure of penetration depth between convex polyhedral bodies for rigid multibody dynamics☆

Gary D. Hart[a], Mihai Anitescu[b]

[a] *University of Pittsburgh at Greensburg, Division of Natural Sciences, 150 Finoli Drive, Greensburg, PA 15601, email* gdhart@pitt.edu
[b] *Mathematics and Computer Science Division, Argonne National Laboratory, 9700 S. Cass Avenue, Argonne, IL 60439, email* anitescu@mcs.anl.gov

Abstract

In this work, we define a new metric of the distance and depth of penetration between two convex polyhedral bodies. The metric is computed by means of a linear program with three variables and $m + n$ constraints, where m and n are the number of facets of the two polyhedral bodies. As a result, this metric can be computed with $O(m + n)$ algorithmic complexity, superior to the best algorithms known for calculating Euclidean penetration depth. Moreover, our metric is equivalent to the signed Euclidean distance and thus results in the same dynamics when used in the simulation of rigid-body dynamics in the limit of the time step going to 0. We demonstrate the use of this new metric in time-stepping methods for rigid body dynamics with contact and friction.

Keywords: rigid body, contact dynamics, friction, measure differential inclusion, complementarity problems

1. Introduction

Rigid multibody dynamics (RMBD) is an important area of mathematical modeling that seeks to predict the position and velocity of a system of rigid bodies. Current research in rock dynamics [32], human motion [11, 28], robotic simulation [37, 38], and virtual reality [21, 30, 31] are just a few of the numerous areas that use RMBD.

Approaches for simulating rigid multibody dynamics with contact and friction have included piecewise differential algebraic equations methods [20], acceleration-force linear complementarity problem methods [12, 16, 36], penalty (or regularization) methods [15, 33], and velocity-impulse, complementarity-based time-stepping methods [2, 5, 8, 10, 29, 34, 35]. While these

☆This paper is based on the Ph.D. thesis of the first author [18]

approaches differ in philosophy, they have one common computational requirement: they need the distance between two bodies, as well as a measure of their depth of penetration should it occur. There exist approaches that ensure that the bodies involved in collision and contact never penetrate [27] and thus need to compute only the distance between bodies and not the penetration depth. Nevertheless, such approaches have significant difficulty in handling other constraints, such as joint constraints. Moreover, ensuring that penetration does not occur in any circumstance requires extremely small time steps, a feature that often limits performance. Allowing for some penetration permits more flexibility in the dynamics resolution and, in particular, permits the development of schemes that proceed at fixed time step [2, 5, 29]. The reason is that collision and contact resolution can be done as a part of the complementarity problem that determines the new velocity. Many other RMBD algorithms allow for some amount of penetration [8, 15, 22, 33].

To allow for penetration, RMBD approaches need the computation of the depth of penetration between two bodies. The metric of the relative configuration of two bodies most commonly used in RMBD that also allows a description of the penetration depth is the Minkowski penetration depth. For convex polyhedral bodies, several good and practical algorithms compute this depth [1, 22, 23]. The reason for focusing on convex polyhedral bodies is that they are possibly the most used primitive shapes in computational geometry for the purpose of simulation; any body can be well approximated by unions of such convex polyhedral bodies. Nevertheless, all algorithms for computing the Minkowski penetration depth have a guaranteed complexity that is superlinear in the total number of facets of the polyhedra. Moreover, for the purposes of RMBD *it is not necessary to use this particular metric*. What is necessary is to define a signed metric of the relative configuration that is 0 when the bodies are in contact, positive when separated, and negative when penetration occurs and that has particular features that make it usable, namely, an ability to efficiently describe and compute its differentiability properties, the key for setting up the dynamics [3], as well as some compatibility between it and the Minkowski penetration depth. This follows from the fact that RMBD is defined only in terms of presence and absence of exact contact. Thus, what is truly needed is a metric that behaves robustly as the dynamics is approximated by means of time discretization, when some amount of penetration could occur. This observation can be used to define more efficient metrics of relative configuration between two bodies that still result in the correct dynamics in the limit of the time step going to 0.

In §2 we introduce such a metric for the amount of separation and penetration between two convex polyhedra bodies. The novel metric is based on a linear program whose constraints are defined in terms of the faces of the polyhedral bodies involved. Following results from complexity theory of linear programming [25], we conclude that the theoretical complexity of computing this metric grows only linearly with the number of faces of the two bodies. Moreover, the metric is equivalent to the Euclidean distance and Minkowski penetration depth [18] and will thus produce the same dynamical trajectories of the simulated system in the limit of the time step going to 0 *with the same asymptotic efficiency*. For such a metric (or any metric) to be usable in a time-stepping algorithm, one needs to compute its (generalized) gradient information, which defines the contact normals, including for possibly inactive contact features. In §3 we describe how this is done for our metric. The key step in computing the generalized gradient information is to decompose the contact configuration in its basic features, which we call *events*. In §4 we describe how the new metric we defined can be included in a time-stepping scheme and we demonstrate in §5 its use in several numerical experiments.

2. The ratio metric

While minimal Euclidean distance between two bodies is a useful metric, it fails to describe the extent of the penetration when it exists. In this case, we can use the Minkowski penetration depth (MPD), the natural extension of the Euclidean minimum distance function, to quantify the penetration depth between two bodies. It is the minimum length of a translation vector that is applied to one of two penetrating bodies that results in the interiors of the displace bodies being disjoint. Let P_1 and P_2 be convex polyhedra. The MPD between the two bodies is defined formally as

$$PD(P_1, P_2) = \min\{\|d\| | interior(P_1 + d) \bigcap P_2 = \emptyset\}.$$

The worst-case deterministic complexity in computing the depth of penetration using MPD is $O(m^2+n^2)$ [1, 23, 24], where m and n, respectively, are the number of faces of P_1 and P_2. Agarwal *et al.* [1] have produced a randomized method for approximating the depth of penetration with complexity of $O(m^{3/4+\epsilon}n^{3/4+\epsilon})$ for any $\epsilon > 0$.

Our goal is to define a new measure that defines the distance between convex polyhedra and whose complexity is only linear in the total number of faces $m + n$.

2.1. Expansion and Contraction Maps

We use the defining inequalities to provide a compact way to describe a convex polyhedron. Then we define the expansion (or contraction) of that polyhedron with respect to a given interior point. We find that there exists a mapping associated with this expansion/contraction, which we also define.

We use the notation CP(A, b, x_o) to be the convex polyhedron P defined by the linear inequalities $Ax \leq b$ with an interior point x_o. We will often just write P = CP(A, b, x_o). Also, for any nonnegative real number t, the expansion (contraction) of P with respect to the point x_o is defined to be

$$P(x_o, t) = \{x | Ax \leq tb + (1 - t)Ax_o\}.$$

If the interior point x_o is obvious or assumed to be known, we will often write P(t), for simplicity of notation. Hart [18] has shown that whenever P = CP(A, b, x_o) has a nonempty interior, then $P(x_o, s) \subseteq P(x_o, t)$ if and only if $s \leq t$. Moreover $P(x_o, t)$ must be convex.

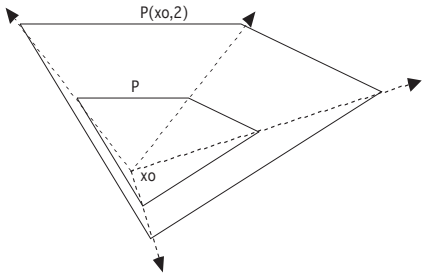

Figure 1: Demonstration of growth

For any value of $t > 0$, $P(x_o, t)$ is a polyhedron similar to P. The faces of $P(x_o, t)$ are parallel to the corresponding faces of P. Also, the expansion (contraction) of P(t) as t increases (decreases)

is linear in every radial direction centered at x_o. In particular, every point on the boundary of $P(x_o, 2)$ is exactly twice as far as the corresponding point of P is from x_o. See Figure 1.

The family of polyhedra $\{P(x_o, t)|t \geq 0\}$ is often described as a concentric family with center x_o. Notice that we always have P(x_o, 1) = P. Notice also that for any value of t ≥ 0, we get $x_o \in P(x_o, t)$. Moreover, P = CP(A, b, x_o) is already closed; thus, if P is bounded, then P(x_o, 0) = x_o.

2.2. Ratio Metric for Polyhedra

We now define a metric based on the simultaneous expansion or contraction of two convex polyhedra. The idea is that two nonintersecting convex polyhedra will simultaneously expand until they reach perfect contact. Likewise, two interpenetrating convex polyhedra will simultaneously contract until they reach perfect contact. In brief, the ratio metric penetration depth captures the amount of expansion or contraction needed to achieve perfect contact.

Definition 1. *Let $P_i = CP(A_i, b_i, x_i)$ be a convex polyhedron for i = 1,2. Then the ratio metric between the two sets is given by*

$$r(P_1, P_2) = \min\{t|P_1(x_1, t) \bigcap P_2(x_2, t) \neq \emptyset\}, \tag{2.1}$$

and the corresponding ratio metric penetration depth (RPM) is given by

$$\rho(P_1, P_2) = \frac{r(P_1, P_2) - 1}{r(P_1, P_2)}. \tag{2.2}$$

Suppose $P_i = CP(A_i, b_i, x_i)$ is a convex polyhedron for i = 1,2. Then $P_i(x_i, 0)$ is always equal to $\{x_i\}$, $P_i(x_i, t)$ is always closed; and, given any point z, we can find a nonnegative real number t_i such that $z \in P_i(x_i, t_i)$. As long as x_1 and x_2 are distinct, the ratio metric between the two sets is well defined, and thus so is the ratio metric penetration depth. We also note the following.

- P_1 and P_2 interpenetrate if and only if $r(P_1, P_2) < 1$ and $\rho(P_1, P_2) < 0$.
- P_1 and P_2 do not intersect if and only if $r(P_1, P_2) > 1$, and $\rho(P_1, P_2) > 0$.
- P_1 and P_2 intersect but do not interpenetrate (they are in perfect contact) if and only if $r(P_1, P_2) = 1$ and $\rho(P_1, P_2) = 0$.

Moreover, since the value returned by the ratio metric is nonnegative, it is impossible for two of our convex polyhedra to have a ratio metric of 0 if their corresponding given interior points are distinct. Also, $r(P_1, P_2) = 0$ if and only if $x_1 = x_2$.

An important issue is the computational complexity of the metric. We note that equation (2.1) is a linear program. Indeed, a reformulation of the definition of r results in

$$r(P_1, P_2) = \min\{t \geq 0 \mid A_i x \leq t b_i + (1 - t) A_i x_i, i = 1, 2\}. \tag{2.3}$$

The linear program has a primal space made of the variables t, x and thus has a dimension of the primal variable space equal to 4 for three-dimensional configurations and 3 for two-dimensional ones. Since our special signed distance function for convex polyhedral bodies is based on solving a linear program, the advantage is that computing this metric function has complexity $O(m + n)$,

where m, n are the number of facets of the polyhedra. This results from the complexity of linear programming when the dimension of the primal variable set is fixed (4 in our case) but the number of constraints is variable [25].

Arguably, other metrics could be defined with the same sign as ρ. Nevertheless, we chose this definition since it simplifies the proof of the metric equivalence theorem, described next.

2.3. Metric Equivalence

Of course, the metric we have defined is different from the Minkowski penetration depth. Nevertheless, for the purpose of using the metric in multibody dynamics, all that is truly needed is for the metric to be compatible with the Euclidean metric, in the sense that if one converges to 0, so should the other. Moreover, since we aim to maintain feasibility in the limit of the time step going to 0, as described in §4, this feature is needed only in a neighborhood of the configurations with perfect contact.

In particular, we will assume that our simulations do not allow too much penetration. To model this restriction, we will choose a parameter $\epsilon \geq 0$ that represents the maximum allowable penetration between any two bodies. With this restriction, we can now state the *metric equivalence theorem*, proved in the Ph.D. thesis of the first author [18].

Theorem 2. *Let $P_i = CP(A_i, b_i, x_i)$ be a convex polyhedron for i = 1,2, s be the MPD between the two bodies (or the Euclidean distance if the two bodies do not penetrate each other); D be the distance between x_1 and x_2; and ϵ be the maximum allowable Minkowski penetration between any two bodies. Then the ratio metric penetration depth (RMPD) between the two sets satisfies the relationship*

$$\frac{s}{D} \leq \rho(P_1, P_2) \leq \frac{s}{\epsilon}.$$

if P_1 and P_2 have disjoint interiors, and

$$-\frac{s}{\epsilon} \leq \rho(P_1, P_2) \leq -\frac{s}{D}$$

if the interiors of P_1 and P_2 are not disjoint.

When h is the step size, the importance of the metric equivalence theorem (2) is that, if a method using RPD is $O(h^p)$, where h is the time step, then so is that method using MPD. Therefore, not only will the MPD noninterpenetration constraints be satisfied by time-stepping schemes based on RPD, but they will have the *same asymptotic order with lower computational complexity*.

3. Differentiability of the ratio metric function

For the mathematical model of polyhedral contact dynamics problems, we need to calculate normal vectors when contact exists [3]. In particular, if the gap function is differentiable, then the normal vector is simply the gradient of the gap function. On the other hand, when the bodies are polyhedral, the gap functions cannot be differentiable. Nevertheless, as we later show, the gap function is piecewise differentiable. In this case, elements of its generalized gradient can be used to generate normal vectors that are used in the same way as for multi-contact configurations. We describe the machinery for this process in this section.

3.1. Perfect Contact

We begin by defining the concept of perfect contact. Two convex polyhedra are said to be in **perfect contact** when there is a nonempty intersection without interpenetration. When two bodies are in perfect contact, the region of contact must lie on the boundary of both bodies.

Definition 3. *In n-dimensional space, a **basic contact unit (BCU)** is any contact that occurs when*

- *two convex polyhedra are in perfect contact,*
- *the contact region attached to a BCU is a point, and*
- *exactly n+1 facets are involved at the contact.*

*The point where the contact occurs is called an **event point**, or more simply, an **event**.*

Notice that when there is perfect contact, regardless of the dimension, the intersection of two convex polyhedra in perfect contact is the convex hull of the event points [18]. In Figure 2, for instance, the contact region is a line segment, that is the convex hull of the two events shown.

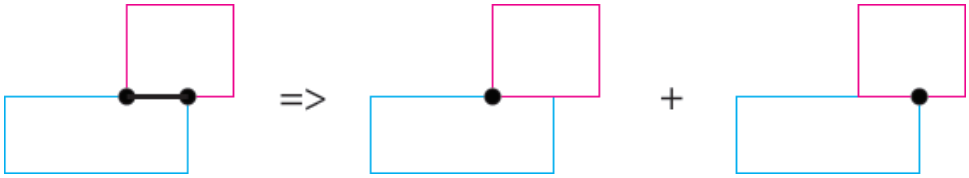

Figure 2: 2D example: contact region is convex hull of BCUs.

Occasionally, at a point of perfect contact, we will simply say that an event occurs. In Figure 2, for instance, we have two point-on-face events occurring.

If $P_i = CP(A_i, b_i, x_i)$ is a convex polyhedron for $i = 1, 2$, and $t^* = r(CP(A_1, b_1, x_1), CP(A_2, b_2, x_2))$, then $P_1(x_1, t^*)$ and $P_2(x_2, t^*)$ are in perfect contact. Let E be any event of this perfect contact. For any $i = 1, 2$, we define the restrictions of $P_i(x_i, t)$ to E, which we denote as $P_E(x_i, t)$, to be the convex body defined by the facets of $P(x_i, t)$ that involve E.

Suppose we have $P_{L_i} = CP(A_{L_i}, b_{L_i}, 0)$ as the local representation for a convex polyhedron for $i = 1, 2$. The transformation from local coordinates x_{L_i} to world coordinates x is given by

$$x = x_i + R_i x_{L_i},$$

which can be rewritten, using typical rotation matrices R_1 and R_2, in the form

$$x_{L_i} = R_i^T (x - x_i).$$

Local formulation of $P_i = CP(A_{L_i}, b_{L_i}, 0)$ is equivalent to global formulation of $P_i = CP(A_{L_i} R_i^T, b_{L_i} + A_{L_i} R_i^T x_i, x_i)$. Hence, our ratio metrics globally become the computation of

$$\begin{aligned} r(P_1, P_2) &= \min_{t \geq 0} \begin{cases} A_{L_1} R_1^T x \leq t(b_{L_1} + A_{L_1} R_1^T x_1) + (1-t) A_{L_1} R_1^T x_1 \\ A_{L_2} R_2^T x \leq t(b_{L_2} + A_{L_2} R_2^T x_2) + (1-t) A_{L_2} R_2^T x_2 \end{cases} \\ &= \min_{t \geq 0} \begin{cases} A_{L_1} R_1^T x - b_1 t \leq A_{L_1} R_1^T x_1 \\ A_{L_2} R_2^T x - b_2 t \leq A_{L_2} R_2^T x_2 \end{cases} . \end{aligned} \tag{3.4}$$

The restrictions $P_E(x_i, t)$ for i = 1,2 which can be written as

$$\hat{A}_{L_i} R_i^T x - \hat{b}_i t \leq \hat{A}_{L_i} R_i^T x_i,$$

where $\hat{A}_i = Q_i A_i$ and $\hat{b}_i = Q_i b_i$ and Q_i is the projection matrix that chooses the inequalities that define the facets of $P(x_i, t)$ that involve E. Therefore

$$r(P_E(x_1, t), P_E(x_2, t)) = \min_{t \geq 0} \left\{ \begin{array}{l} \hat{A}_{L_1} R_1^T x - \hat{b}_1 t \leq \hat{A}_{L_1} R_1^T x_1 \\ \hat{A}_{L_2} R_2^T x - \hat{b}_2 t \leq \hat{A}_{L_2} R_2^T x_2 \end{array} \right. \tag{3.5}$$

where the sum of the rows of $\hat{A}_{L_1}$ and $\hat{A}_{L_2}$ totals n+1.

We note that a combination of facets for which the calculation of (3.5) will be identical to (3.4) yields an event point caused when the bodies are in perfect contact. The significance of this is that there are finitely many combinations of interest, and that leads us to examine the implicit piecewise definition of our metric.

3.2. Component Signed Distance Functions

The gradient is used to produce the normal vectors at contact between two bodies. For the global formulation of $P_i = CP(A_{L_i} R_i^T, b_{L_i} + A_{L_i} R_i^T x_i, x_i)$ for $i = 1, 2$, we can list all the potential events. Suppose that there are $n_{1,2}$ such potential events. We will use the component functions corresponding to each potential event.

We associate with the m^{th} potential event $E^{(m)}$, a component function $\widehat{\Phi}^{(m)}$, and we use the restrictions $P_{E^{(m)}}(x_1, t)$ and $P_{E^{(m)}}(x_2, t)$. Then we write $\widehat{\Phi}^{(m)}$ in the form $\widehat{\Phi}^{(m)} = f(r_m)$, where $f(t) = (t-1)/t$ and

$$r_m = \min_{t \geq 0} \left\{ \begin{array}{l} \hat{A}_{m_1} R_1^T x - b_{m_1} t \leq \hat{A}_{m_1} R_1^T x_1 \\ \hat{A}_{m_2} R_2^T x - b_{m_2} t \leq \hat{A}_{m_2} R_2^T x_2 \end{array} \right. ,$$

where the sum of the numbers of rows of $\hat{A}_{m_1}$ and $\hat{A}_{m_2}$ is n+1.

Notice that $\widehat{\Phi}^{(m)}$ depends on the translation and rotation variables. Also note that $\widehat{\Phi}^{(m)}$ might not be defined. Indeed, we expect $\widehat{\Phi}^{(m)}$ to be defined for some configurations of the global position variables, and not defined for others, in which cases we consider $\widehat{\Phi}^{(m)}$ to have the value of $-\infty$ for convenience. The following theorem, due to Hart [18] tells us that the ratio metric penetration depth is the maximum of component distance functions. It will play a key role in the computation of the generalized gradient.

Theorem 4. *Suppose $x_1 \neq x_2$. Let $P_i = CP(A_{L_i} R_i^T, b_{L_i} + A_{L_i} R_i^T x_i, x_i)$ be convex polyhedra for $i = 1, 2$, and let $\left\{E^{(1)}, E^{(2)}, \cdots, E^{(N)}\right\}$ be the list of all possible events with corresponding component distance functions $\left\{\widehat{\Phi}^{(1)}, \widehat{\Phi}^{(2)}, \cdots, \widehat{\Phi}^{(N)}\right\}$. Then*

$$\rho(P_1, P_2) = \max\left\{\widehat{\Phi}^{(1)}, \widehat{\Phi}^{(2)}, \cdots, \widehat{\Phi}^{(N)}\right\},$$

where $\rho(P_1, P_2)$ is defined by (2.2).

3.3. Differentiability Restricted at Perfect Contact

It is unreasonable to expect the ratio metric to be differentiable at a point of contact that is not a BCU, just as it is unreasonable to expect a real-valued function of a real variable to be

differentiable when its graph has a corner. In this case the nonuniqueness of a potential normal vector is the problem.

Suppose that we have two convex polyhedra in perfect contact. When we restrict ourselves to any event that occurs because of this perfect contact, the ratio metric (and thus the ratio metric penetration depth) needs to be differentiable. A theorem due to Hart [18], in fact, states that for convex polyhedra $P_i = CP(A_{L_i}R_i^T, b_{L_i} + A_{L_i}R_i^T x_i, x_i)$ in world coordinates for $i = 1, 2$, at any event of perfect contact E, $r(P_E(x_1, t), P_E(x_2, t))$ is infinitely differentiable with respect to the translation vectors and rotation angles.

We thus conclude that the component functions $\widehat{\Phi}^{(m)}$ are *infinitely differentiable* if they are active perfect contact events. We call a component function active if $\widehat{\Phi}^{(m)} = \rho(P_1, P_2)$. An immediate open set argument shows that *nearly active* perfect contact events also have $\widehat{\Phi}$ infinitely differentiable with respect to the translation vectors and rotation angles.

Therefore, when all component functions correspond to perfect contact events, the function ρ is piecewise smooth. In the next subsection, we describe how its generalized gradient can then be computed.

3.4. Generalized Gradient of the Ratio Metric

We now list one of the assumptions about the kinematic description of the non-interpenetration constraints.

Assumption A1: There exist $\epsilon_o > 0$, $C_1^d > 0$, and $C_2^d > 0$ such that

- $\Phi^{(j)}$ for $1 \leq j \leq n_B$ are piecewise continuous on their domains Ω_ϵ, with piecewise components $\widehat{\Phi}^{(m)}(q)$, which are twice continuously differentiable in their respective open domains with first and second derivatives uniformly bounded by $C_1^d > 0$ and $C_2^d > 0$, respectively, and
- $\Theta^{(i)}(q)$ for $i = 1, 2, \cdots, m$ are twice continuously differentiable in Ω_ϵ with first and second derivatives uniformly bounded by $C_1^d > 0$ and $C_2^d > 0$, respectively.

Let us now prove a small lemma concerning the representation of our piecewise functions on a line segment.

Lemma 5. *Let the functions $\Phi^{(j)}$ be piecewise continuously differentiable. Also, let the position q, the vector w, and real number $t > 0$ be given such that the line segment from q to $q + tv$ is feasible. Then we can find a sequence $\left\{t_1, t_2, \ldots, t_{k_j}\right\}$ of increasing positive real numbers and a sequence of component functions $\left\{\hat{\Phi}^{(m_1)}, \hat{\Phi}^{(m_2)}, \ldots, \hat{\Phi}^{(m_{k_j})}\right\}$ such that*

$$\Phi^{(j)}(q + tv) - \Phi^{(j)}(q) = \sum_{i=1}^{k_j} \left[\hat{\Phi}^{(m_i)}(q + t_i v) - \hat{\Phi}^{(m_i)}(q + t_{i-1} v)\right]. \tag{3.6}$$

Proof. Since we know that the segment from q to $q + tv$ is in the domain of $\Phi^{(j)}$, we consider that very segment which we will subdivide into finitely many subsegments.

Let $t_o = 0$. At the point p, there is an active event, m_1. We can then find t_1 which is the largest value of t for which m_1 is active. If $q + t_1 v$ is not equal to $q + tv$, then we repeat the process, finding an active event m_2 at $q + t_1 v$ and the largest value of t, say t_2 with $t_2 > t_1$, for which m_2 is active.

Because of the unique way $\Phi^{(j)}$ is defined, the way we defined the t_i, and the fact that only finitely many events exist, we can use Theorem 4 to enumerate a finite number of values $t_1, t_2, \ldots, t_{k_j}$ and associated events $m_1, m_2, \ldots, m_{k_j}$ such that on the i^{th} segment we get

$$\Phi^{(j)}(q + tv) = \hat{\Phi}^{(m_i)}(q + tv) \quad \forall t \in [t_{i-1}, t_i].$$

We can then write

$$\begin{aligned} \Phi^{(j)}(q + tv) - \Phi^{(j)}(q) &= \sum_{i=1}^{k_j} \left[\Phi^{(j)}(q + t_i v) - \Phi^{(j)}(q + t_{i-1} v)\right] \\ &= \sum_{i=1}^{k_j} \left[\hat{\Phi}^{(m_i)}(q + t_i v) - \hat{\Phi}^{(m_i)}(q + t_{i-1} v)\right], \end{aligned} \tag{3.7}$$

which completes the proof. □

Lemma 6. *If Assumption A1 holds, then for any j such that $1 \leq j \leq n_B$, we have $\Phi^{(j)}$ is everywhere directionally differentiable. Moreover, the generalized gradient of $\Phi^{(j)}$ is contained in the convex cover of the gradients of its component functions that are active at q and evaluated at q.*

Proof. Let q be any point in the domain of $\Phi^{(j)}$. We need to consider the generalized directional derivative of $\Phi^{(j)}$ at q in the direction v is defined (see [13]) by

$$\Phi^{(j)^o}(q; v) = \limsup_{p \to q, t \downarrow 0} \frac{\Phi^{(j)}(p + tv) - \Phi^{(j)}(p)}{t}.$$

We therefore consider the segment from q to $q + tv$, which we will subdivide into finitely many subsegments.

We invoke Lemma 5 so that from p to $p + \tau w$ for $0 \leq \tau \leq t$, we can find an increasing sequence of values $0 = t_o < t_1 < \cdots < t_n = t$ and corresponding restrictions $\hat{\Phi}^{(m_i)}$.

Next we use differentiability of the component functions and the mean value theorem to calculate

$$\begin{aligned} \tfrac{1}{t}\left[\Phi^{(j)}(p + tv) - \Phi^{(j)}(p)\right] &= \frac{1}{t} \sum_{i=1}^{k} \left[\hat{\Phi}^{(m_i)}(p + t_i v) - \Phi^{(j)}(p + t_{i-1} v)\right] \\ &= \frac{1}{t} \sum_{i=1}^{k} \left[(t_i - t_{i-1}) \nabla \hat{\Phi}^{(m_i)^T}(p + \zeta_{i-1} v) v\right]. \end{aligned}$$

Since we know that

$$\limsup_{p \to q, t \downarrow 0} \nabla \hat{\Phi}^{(m_i)}(p + \zeta_{i-1} v) = \nabla \hat{\Phi}^{(m_i)}(q)$$

and

$$\lim_{t \to 0} \frac{1}{t} \sum_{i=1}^{k} (t_i - t_{i-1}) = 1,$$

our initial calculation can be simplified because the calculation of $\Phi^{(j)^o}(q; v)$ always produces a convex combination of the gradients of the events that are active at q and evaluated at q. This is enough to show that the generalized gradient $\partial \Phi^{(j)}(q)$ must be contained within the convex cover of the gradients of the component functions that are active at q and evaluated at q. □

Lemma 7. *If Assumption A1 holds, then for any j such that $1 \leq j \leq n_B$, $\Phi^{(j)}$ satisfies a Lipschitz condition.*

Proof. By Lebourg's mean value theorem [13], given q_1 and q_2 in the domain of $\Phi^{(j)}$, there exists q_o on the line segment between q_1 and q_2 that satisfies

$$\Phi^{(j)}(q_1) - \Phi^{(j)}(q_2) \in \left\langle \partial\Phi^{(j)}(q_o), q_1 - q_2 \right\rangle.$$

Hence, there is some $\Gamma \in \partial\Phi^{(j)}$ such that

$$\Phi^{(j)}(q_1) - \Phi^{(j)}(q_2) = \Gamma(q_1 - q_2).$$

However, we know by Lemma 6 that Γ must be a convex combination of gradients of component functions. Notice that by Assumption A1, each of these gradients can be bounded above by C_1^d. Thus, we must have

$$\left|\Phi^{(j)}(q_1) - \Phi^{(j)}(q_2)\right| \leq C_1^d \|q_1 - q_2\|,$$

which concludes the proof. □

4. The time-stepping algorithm

We will often use complementarity notation which, we now define.

Definition 8. *Let a and b be real numbers satisfying the following.*

1. $a \geq 0$
2. $b \geq 0$
3. $ab = 0$

Then a and b are complementary. We say that a and b satisfy a complementarity condition, and we write

$$a \geq 0 \perp b \geq 0.$$

The vectors u and v of length k satisfy a complementarity condition if $u^{(i)}$ is complementary to $v^{(i)}$ for $i = 1, 2, \ldots, k$. We denote the condition by

$$u \geq 0 \perp v \geq 0.$$

As we model the motion, we have to observe constraints, whether implicit or explicit, if our model is to be realistic. Geometrical constraints involve only the position variable and depend on the shape of the bodies and the type of constraints involved. We focus our attention on noninterpenetration constraints, a geometrical condition, and on the kinematic friction constraint. The translational and angular components of a body are commonly grouped into one vector, which we call the composite position [20]. In what follows, we use a vector q to represent the composite position of a body.

Polyhedral Bodies. Our model assumes that all bodies are convex and polyhedral. For the j_i^{th} body, we define $P_{j_i} = CP(A_{j_j}, b_{j_i}, 0)$ to be the polyhedron defined by the linear inequalities

$$A_{j_i} x \leq b_{j_i},$$

which contains the origin. By convention and without loss of generality, we normalize this system such that all entries of vector b_{j_i} are equal to 1.

Rotation Matrix. Suppose that the position of the body B_{j_i} has center at x_{j_i} and rotation angles θ_{j_i}. Using world coordinates, we get $P_{j_i} = CP(A_{j_i}R^T_{j_i}(\theta_{j_i}), b_{j_i} + A_{j_i}R^T_{j_i}(\theta_{j_i})x_{j_i}x_{j_i})$. Here R_{j_i} is a rotation matrix. We will use an Euler angle parameterization of the rotation matrix.

Position Coordinates. Let the space Q_j contain the generalized coordinates for the bodies B_{j_1} and B_{j_2}. This is accomplished if the bodies B_{j_1} and B_{j_2} have centers at x_{j_1} and x_{j_2}, respectively, and respective rotation angles θ_{j_1} and θ_{j_2}. Then the generalized position vector in Q_j is

$$q_j = \begin{bmatrix} x_{j_1} \\ \theta_{j_1} \\ x_{j_2} \\ \theta_{j_2} \end{bmatrix}.$$

Now suppose that we have n_B rigid bodies in the system. Denote by $Q_1, Q_2, \ldots, Q_{n_B}$ the spaces that contain generalized coordinates of the bodies $B_1, B_2, \ldots, B_{n_B}$, whose generalized coordinates we denote by $q_1, q_2, \ldots, q_{n_B}$. These spaces are locally homeomorphic with some bounded open set of R^s [20]. The aggregate generalized position (from here on, the generalized position) becomes $q = (q_1^T, q_2^T, \ldots, q_{n_B}^T)^T$. We denote $Q = Q_1 \times Q_2 \times \ldots, Q_{n_B}$.

4.1. Physical Constraints

Physically, we need to constrain the bodies from penetrating one another if they are not to occupy the same space. Additionally, we need to describe how we model contact and how we handle friction.

Noninterpenetration Constraints. Typically, mathematical models of the constraints of noninterpenetration are defined in terms of a continuous signed distance function between the two bodies $\Phi^{(j)}(q)$ [3]. We will write the collection of these noninterpenetration constraints as

$$\Phi^{(j)}(q) \geq 0, \quad j = 1, 2, \ldots, p.$$

Our model computes the ratio metric penetration depth as the signed distance functions between the piecewise smooth polyhedra P_{j_1} and P_{j_2} using Definition 1. If the bodies B_{j_1} and B_{j_2} have centers at x_{j_1} and x_{j_2}, respectively, and respective rotation angles θ_{j_1} and θ_{j_2}, then at the generalized position q we have

$$\Phi^{(j)}(q) = \rho(P_{j_1}, P_{j_2}) = \frac{r(P_{j_1}, P_{j_2}) - 1}{r(P_{j_1}, P_{j_2})},$$

where

$$r(P_{j_1}, P_{j_2}) = \min\{t | P_{j_1}(x_{j_1}, t) \bigcap P_{j_2}(x_{j_2}, t) \neq \emptyset\}.$$

We will refer to the $\Phi^{(j)}(q)$ simply as the *(signed) distance functions*. It should be clear that these distance functions are mappings that depend continuously on q and on the shape of the bodies, but we consider the latter dependency only implicitly.

Sufficient conditions for local differentiability of $\Phi^{(j)}(q)$ have been discussed in [5]. For our polyhedral bodies, however, the function $\Phi^{(j)}(q)$ cannot be differentiable everywhere. We earlier discussed the fact that our distance function is piecewise differentiable. We need to take advantage of this piecewise differentiability.

Suppose that the j^{th}signed distance function $\Phi^{(j)}(q)$ will have k_j component signed distance functions.

$$\Phi_1^{(j)}(q), \Phi_2^{(j)}(q), \ldots, \Phi_{k_m}^{(j)}(q), \quad j = 1, 2, \ldots, p.$$

For convenience, we rename the collection of component as

$$\widehat{\Phi}^{(m)}(q), \quad m = 1, 2, \ldots, p_o,$$

where $p_o = k_1 + k_2 + \cdots + k_p$.

At any event E at the perfect contact, our model uses the restrictions $P_E(x_{j_i}, t)$ for $i = 1, 2$ to compute $r(P_E(x_{j_1}, t), P_E(x_{j_2}, t))$, with which we define the component function

$$\widehat{\Phi}^{(m)}(q) = \frac{r(P_E(x_{j_1}, t), P_E(x_{j_2}, t))) - 1}{r(P_E(x_{j_1}, t), P_E(x_{j_2}, t))}.$$

Contact Model. We now denote the normal at an event (m) by

$$n^{(m)}(q) = \nabla_q \widehat{\Phi}^{(m)}(q), \quad m \in \mathcal{E}.$$

When the contact is active, it can exert a compressive normal impulse, $c_n^{(m)} n^{(m)}(q)$, on the system, which is modeled mathematically by requiring $c_n^{(m)} \geq 0$. The fact that the contact must be active before a nonzero compression impulse can act is expressed by the complementarity constraint

$$[h]\widehat{\Phi}^{(m)}(q) \geq 0 \perp c_n^{(m)} \geq 0, \quad m \in \mathcal{E}. \tag{4.8}$$

See Figure 3 for an illustration of the model of contact..

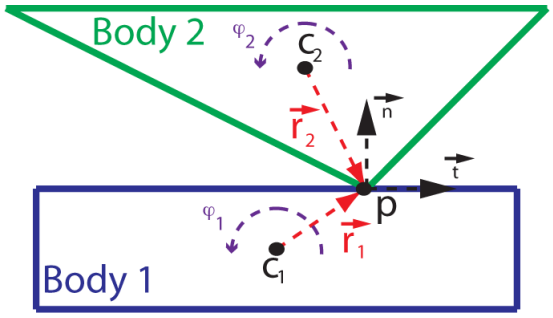

Figure 3: Model of contact

Friction Constraints. Frictional constraints are expressed by means of a discretization of the Coulomb friction cone [8, 9, 35]. For a contact $m \in \{1, 2, \ldots, p_o\}$, we take a collection of coplanar vectors $d_i^{(m)}(q)$, $i = 1, 2, \ldots, M_C^{(m)}$, which span the plane tangent at the contact (though the plane may cease to be tangent to the contact normal when mapped in generalized coordinates [3]). The convex cover of the vectors $d_i^{(m)}(q)$ should approximate the transversal shape of the friction cone.

Denote by $D^{(m)}(q)$ a matrix whose columns are $d_i^{(m)}(q) \neq 0$, $i = 1, 2, \ldots, M_C^{(m)}$, that is, $D^{(m)}(q) = \left[d_1^{(m)}(q), d_2^{(m)}(q), \ldots, d_{M_C^{(m)}}^{(m)}(q)\right]$. A tangential impulse is $\sum_{i=1}^{M_C^{(m)}} \beta_i^{(m)} d_i^{(m)}(q)$, where $\beta_i^{(m)} \geq 0$, $i = 1, 2, \ldots, M_C^{(m)}$. Assume that the tangential contact description is balanced, that is,

$$\forall i,\ 1 \le i \le M_C^{(m)},\ \exists k,\ 1 \le k \le M_C^{(m)} \text{ such that } d_i^{(m)}(q) = -d_k^{(m)}(q).$$

The friction model requires maximum dissipation for given normal impulse $c_n^{(m)}$ and velocity v and guarantees that the total contact force is inside the discretized cone. This model can be expressed as

$$\begin{array}{rcccl} D^{(m)^T}(q)v + \lambda^{(m)}e^{(m)} & \ge 0 & \perp & \beta^{(m)} \ge 0, \\ \mu c_n^{(m)} - e^{(m)^T}\beta^{(m)} & \ge 0 & \perp & \lambda^{(m)} \ge 0. \end{array} \tag{4.9}$$

Here $e^{(m)}$ is a vector of ones of dimension $M_C^{(m)}$, $e^{(m)} = (1, 1, \ldots, 1)^T$, $\mu^{(m)} \ge 0$ is the Coulomb friction parameter, and $\beta^{(m)}$ is the vector of tangential impulses $\beta^{(m)} = \left(\beta_1^{(m)}, \beta_2^{(m)}, \ldots, \beta_{M_C^{(m)}}^{(m)}\right)^T$. The additional variable $\lambda^{(m)} \ge 0$ is approximately equal to the norm of the tangential velocity at the contact, if there is relative motion at the contact, or $\|D(q)^{(m)^T} v\| \ne 0$ [8, 35].

Linear Complementarity Model. Let $h_l > 0$ be the time step at time $t^{(l)}$, when the system is at position $q^{(l)}$ and velocity $v^{(l)}$. We have that $h_l = t^{(l+1)} - t^{(l)}$. Choose the new position to be $q^{(l+1)} = q^{(l)} + h_l v^{(l+1)}$, where $v^{(l+1)}$ is determined by enforcing the simulation constraints.

The noninterpenetration constraints are enforced at the velocity level by modified linearization of the mappings $\widehat{\Phi}^{(m)}$. At the velocity level, we enforce the noninterpenetration constraint of index j, that is, $\Phi^{(j)}(q) \ge 0$. Thus, modified linearization at $q^{(l)}$ for one time step amounts to $\gamma\Phi^{(j)}(q^{(l)}) + h_l \nabla_q \Phi^{(j)^T}(q^{(l)})v^{(l+1)} \ge 0$, where γ is a user-defined parameter. If $\gamma = 1$, then we would achieve proper linearization, which is the case treated in [5].

Since our noninterpenetration constraints are piecewise defined, we need to have $\widehat{\Phi}^{(m)}(q^{(l)}) \le \Phi^{(j)}(q^{(l)})$. Thus, our linearization becomes $\gamma\Phi^{(j)}(q^{(l)}) + h_l \nabla_q \widehat{\Phi}^{(m)^T}(q^{(l)})v^{(l+1)} \ge 0$; that is, after including the complementarity constraints (4.8) and using the definition of $n^{(m)}(q^{(l)}) = \nabla_q \widehat{\Phi}^{(m)}(q^{(l)})$, we have

$$n^{(m)^T}(q^{(l)})v^{(l+1)} + \frac{\gamma}{h_l}\Phi^{(j)}(q^{(l)}) \ge 0 \perp c_n^{(m)} \ge 0. \tag{4.10}$$

Now we completely define the prevailing system that describes our model. We first use an Euler discretization of the equations of motion, that is, of Newton's law. This results in the following equation [6]:

$$M(q^{(l)})\left(v^{(l+1)} - v^{(l)}\right) \quad = \quad h_l k\left(t^{(l)}, q^{(l)}, v^{(l)}\right) + \sum_{m \in \mathcal{E}} \left(c_n^{(m)} n^{(m)}(q^{(l)}) + \sum_{i=1}^{M_C^{(m)}} \beta_i^{(m)} d_i^{(m)}(q^{(l)}) \right).$$

Next, we use the modified linearization of the noninterpenetration constraints (4.10) to get

$$n^{(m)^T}(q^{(l)})v^{(l+1)} + \tfrac{\gamma}{h_l}\widehat{\Phi}^{(m)}(q^{(l)}) \quad \ge 0 \quad \perp c_n^{(m)} \ge 0, \quad m \in \mathcal{E}.$$

Finally, we include the conditions for model of friction (4.9).

$$\begin{array}{rcccll} D^{(m)^T}(q)v + \lambda^{(m)}e^{(m)} & \ge 0 & \perp & \beta^{(m)} \ge 0 & m \in \mathcal{E}, \\ \mu c_n^{(m)} - e^{(m)^T}\beta^{(m)} & \ge 0 & \perp & \lambda^{(m)} \ge 0 & m \in \mathcal{E}. \end{array}$$

We can then rewrite the system to obtain the following mixed linear complementarity problem:

$$\begin{bmatrix} M^{(l)} & -\widetilde{n} & -\widetilde{D} & 0 \\ \widetilde{n}^T & 0 & 0 & 0 \\ \widetilde{D}^T & 0 & 0 & \widetilde{E} \\ 0 & \widetilde{\mu} & -\widetilde{E}^T & 0 \end{bmatrix} \begin{bmatrix} v^{(l+1)} \\ c_n \\ \widetilde{\beta} \\ \lambda \end{bmatrix} + \begin{bmatrix} -Mv^{(l)} - h_l k^{(l)} \\ \Delta \\ 0 \\ 0 \end{bmatrix} = \begin{bmatrix} 0 \\ \widetilde{\rho} \\ \widetilde{\sigma} \\ \zeta \end{bmatrix} \tag{4.11}$$

$$\begin{bmatrix} c_n \\ \widetilde{\beta} \\ \lambda \end{bmatrix}^T \begin{bmatrix} \widetilde{\rho} \\ \widetilde{\sigma} \\ \zeta \end{bmatrix} = 0, \qquad \begin{bmatrix} c_n \\ \widetilde{\beta} \\ \lambda \end{bmatrix} \geq 0, \qquad \begin{bmatrix} \widetilde{\rho} \\ \widetilde{\sigma} \\ \zeta \end{bmatrix} \geq 0\,. \tag{4.12}$$

Here

$$\begin{aligned} \widetilde{n} &= [n^{(m_1)}, n^{(m_1)}, \ldots, n^{(m_s)}], \\ c_n &= [c_n^{(m_1)}, c_n^{(m_2)}, \ldots, c_n^{(m_s)}]^T, \\ \widetilde{\beta} &= [\beta^{(m_1)T}, \beta^{(m_2)T}, \ldots, \beta^{(m_s)T}]^T, \\ \widetilde{D} &= [D^{(m_1)}, D^{(m_2)}, \ldots, D^{(m_s)}], \\ \lambda &= [\lambda^{(m_1)}, \lambda^{(m_2)}, \ldots, \lambda^{(m_s)}]^T, \\ \widetilde{\mu} &= diag(\mu^{(m_1)}, \mu^{(m_2)}, \ldots, \mu^{(m_s)})^T, \\ \Delta &= \gamma \tfrac{1}{h} \left(\Phi^{(Bod(E^{(m_1)}))}, \Phi^{(Bod(E^{(m_2)}))}, \ldots, \Phi^{(Bod(E^{(m_s)}))}\right)^T, \end{aligned}$$

and

$$\widetilde{E} = \begin{bmatrix} e^{(m_1)} & 0 & 0 & \ldots & 0 \\ 0 & e^{(m_2)} & 0 & \ldots & 0 \\ \vdots & \vdots & \vdots & \vdots & \vdots \\ 0 & 0 & 0 & \ldots & e^{(m_s)} \end{bmatrix}$$

are the lumped LCP data, and $\mathcal{E} = \{m_1, m_2, \ldots, m_s\}$ are the active events constraints. Here $e^{(j)}$ is a vector of ones of dimension $m_C^{(j)}$; that is, $e^{(j)} = (1, 1, \ldots, 1)^T$. The vector inequalities in (4.12) are to be understood componentwise.

To simplify the presentation we do not explicitly include the dependence of the parameters in (4.11–4.12) on $q^{(l)}$. Also, $M^{(l)} = M(q^{(l)})$ is the value of the mass matrix at time $t^{(l)}$, and $k^{(l)} = k(t^{(l)}, q^{(l)}, v^{(l)})$ represents the external force at time $t^{(l)}$.

4.2. Active Set and Active Events

Given the position q, two bodies are in physical contact if and only if $\Phi^{(j)}(q) = 0$ for some j, $1 \leq j \leq p$. We define the physically active set as

$$\left\{ j \mid \Phi^{(j)}(q) = 0, j = 1, \ldots, p \right\}. \tag{4.13}$$

Because of the components of $\Phi^{(j)}(q)$, this is equivalent to having $\Phi_k^{(j)}(q) = 0$, for some j, $1 \leq j \leq p$ and for some k, $1 \leq k \leq k_p$. Since we renamed and reordered the functions, we know that if two bodies are in physical contact, then for some index m, $1 \leq m \leq p_o$, we have $\widehat{\Phi}^{(m)}(q) = 0$.

We need a way to identify where the contact occurs, so in the following, when we refer to *contact j*, we are saying that the two bodies whose (piecewise) distance is determined by $\Phi_k^{(j)}$ are in contact and, because of renaming, we have $\widehat{\Phi}^{(m)} = \Phi_k^{(j)}$. If two bodies are in contact at position q, then $\Phi^{(j)}(q) = \Phi_k^{(j)}(q) = 0$, and hence $\widehat{\Phi}^{(m)}(q) = 0$ for some m.

For computational efficiency, only the events that are imminently active are included in the dynamical resolution and linearized, and their set is denoted by $\mathcal{E}$. One practical way of determining $\mathcal{E}$ is by choosing sufficiently small parameters $\hat{\epsilon}_t$ and $\hat{\epsilon}_x$. The definition becomes

$$
\begin{aligned}
\mathcal{E}_1(q) &= \left\{m \mid \Phi^{(j)} \le \hat{\epsilon}_t,\ j = Bod(E^{(m)}),\ 1 \le m \le p_o\right\} \\
\mathcal{E}_2(q) &= \left\{m \mid 0 \le \widehat{\Phi}^{(m)} - \Phi^{(j)} \le \hat{\epsilon}_t,\ j = Bod(E^{(m)}),\ 1 \le m \le p_o\right\} \\
\mathcal{E}_3(q) &= \left\{m \mid E_x^{(m)} \in CP(A_{L_{m_1}} R_{m_2}^T, b_{L_{m_1}} + A_{L_{m_1}} R_{m_1}^T x_{m_1}, x_{m_1}) + \hat{\epsilon}_x,\ 1 \le m \le p_o\right\} \\
\mathcal{E}_4(q) &= \left\{m \mid E_x^{(m)} \in CP(A_{L_{m_2}} R_{m_2}^T, b_{L_{m_2}} + A_{L_{m_2}} R_{m_2}^T x_{m_2}, x_{m_2}) + \hat{\epsilon}_x,\ 1 \le m \le p_o\right\}
\end{aligned}
$$

and

$$\mathcal{E}(q) = \mathcal{E}_1(q) \bigcap \mathcal{E}_2(q) \bigcap \mathcal{E}_3(q) \bigcap \mathcal{E}_4(q). \tag{4.14}$$

This defines the nearly active (or computationally active) set of events.

The nearly active set of events is related to the nearly active set of contacts. We formally define the computationally active set (or nearly active set) of contacts.

$$\mathcal{A}(q) = \left\{j \mid \Phi^{(j)}(q) \le \hat{\epsilon}_t, j = 1, \ldots, p\right\}, \tag{4.15}$$

where $\epsilon_t > 0$ is a given parameter.

Let a position q be given. If $\mathcal{A}(q)$ is empty, then by definition $\mathcal{E}(q)$ must be empty. On the other hand, if $\mathcal{A}(q)$ is not empty, then at least one event must be active, and so $\mathcal{E}(q)$ cannot be empty. In other words, we have shown that

$$\mathcal{A}(q) = \emptyset \quad \Longleftrightarrow \quad \mathcal{E}(q) = \emptyset.$$

In fact, when $\mathcal{A}(q)$ is not empty, there is some event m such that $\Phi^{(j)}(q) = \widehat{\Phi}^{(m)}(q)$. We cannot have an m such that $\widehat{\Phi}^{(m)}(q) < \Phi^{(j)}(q)$, because then $m \notin \mathcal{E}_2(q)$. The consequence is that

$$\min_{j \in \mathcal{A}} \Phi^{(j)}(q) = \min_{m \in \mathcal{E}} \widehat{\Phi}^{(m)}(q).$$

4.3. Algorithm

Many researchers have pursued a simulate-detect-restart approach [8, 12, 14, 35], where the simulation is stopped at the collision, the collision is often resolved by using, say, LCP techniques [8, 17], and then the simulation is restarted. If many collisions occur per unit of simulation, then there will be many costly updates – or worse, the timestep may easily approach zero in the face of multiple collisions.

In the approach presented here, the active set $\mathcal{A}$ (4.15) is always defined; and with the appropriately chosen parameter $\hat{\epsilon}$, we can compute the computationally active events $\mathcal{E}$ (4.15). Also, for appropriately chosen step size h_l and parameter $\hat{\epsilon}$, our time-stepping scheme may proceed despite small interpenetrations, and the physically active set at the end of each step is contained in $\mathcal{E}$. Thus there is no need to stop the simulation if $\hat{\epsilon}$ is appropriately chosen.

Computationally, our approach is more appealing because we solve only one LCP for fixed time-step h, making it more attractive for interactive simulation. In [4] we showed for the smooth case that this scheme achieves constraint stabilization and that infeasibility at step l is upper bounded by $O(\|h_{l-1}\|^2 \|v^{(l)}\|^2)$. We will show that constraint stabilization is achieved for our piecewise smooth distance functions.

Algorithm 9. Time-Stepping Algorithm for Convex Polyhedra

Algorithm for piecewise smooth multibody dynamics

Step 1: Given $q^{(l)}$, $v^{(l)}$, and h_l, calculate the active set $\mathcal{A}\left(q^{(l)}\right)$ and active events $\mathcal{E}\left(q^{(l)}\right)$.

Step 2: Compute $v^{(l+1)}$, the velocity solution of the mixed LCP (4.11).

Step 3: Compute $q^{(l+1)} = q^{(l)} + h_l v^{(l)}$.

Step 4: IF finished, THEN stop, ELSE set $l = l + 1$ and restart.

We make the following additional assumptions about the kinematic description of the noninterpenetration constraints.

Assumption D1: The mass matrix is constant. That is, $M\left(q^{(l)}\right) = M^{(l)} = M$.

Assumption D2: The norm growth parameter $c(\cdot, \cdot, \cdot)$ used in [5] is constant. That is,

$$c\left(A(q, \widetilde{\mu}), B(q).M\right) \leq c_o \quad \forall \epsilon \in [0, \epsilon_o] \quad \forall q \in \Omega_\epsilon,$$

where $A(q, \widetilde{\mu})$ and $B(q)$ are the matrices defining the inequality constraints and equality constraints, respectively.

Assumption D3: The external force is continuous and increases at most linearly with the position and velocity, and is uniformly bounded in time. That is,

$$k(t, v, q) = k_o(t, v, q) + f_c(v, q) + k_1(v) + k_2(q), \tag{4.16}$$

and there is some constant $c_K \geq 0$ such that

$$\begin{array}{rcl} \|k_o(t, v, q)\| & \leq & c_K \\ \|k_1(v)\| & \leq & c_K \|v\| \\ \|k_2(q)\| & \leq & c_K \|q\|. \end{array}$$

In addition, assume that

$$v^T f_c(v, q) = 0 \quad \forall v, q.$$

We can now state our main results on the constraint stability of our algorithm which can be summarized in the next theorem, which Hart [18] proved.

Theorem 10. *Consider the time-stepping algorithm defined above and applied over a finite time interval [0, T]. Assume the following.*

- *The active set $\mathcal{A}(q)$ is defined by (4.15).*
- *The active events $\mathcal{E}(q)$ are defined by (4.14).*
- *The time steps $h_l > 0$ satisfy*

$$\sum_{l=0}^{N-1} h_l = T, \quad l = 1, 2, \ldots, N-1,$$

$$\frac{h_{l-1}}{h_l} = c_h, \quad l = 1, 2, \ldots, N-1\,.$$

- *The system satisfies Assumptions D1 - D3.*

- *The system is initially feasible. That is,* $I(q^{(0)}) = 0$.

Then, there exist $H > 0$, $V > 0$, *and* $C_c > 0$ *such that*

1. $\|v^{(l)}\| \leq V \ \forall l, 1 \leq l \leq N$, *and*
2. $I\,(q(l)) \leq C_c \|v^{(l)}\|^2 h_{l-1}^2, \forall l, 1 \leq l \leq N$.

At this point, we know that if we can successfully compute the velocity solution of the mixed LCP (4.11) we can implement this solution into Algorithm 9, then, under modest additional assumptions, Theorem 10 will guarantee success.

5. Numerical Results

We now describe computational experiments with the algorithm we presented in §4, which is the algorithm for [7, 19] adapted to the case where we have polyhedral bodies. An application of this method was used in a robotic grasp simulator [26]. We have created several configurations to be simulated.

5.1. Problem: Balance2

The Balance2 problem is two dimensional and has six bodies: two triangles, three squares, and one rectangle. With two squares and a triangle place on the rectangle and delicately balanced on the other triangle, a square is dropped at one end, disturbing the initial balance of the system.

We ran the simulation for 12 seconds. In Figure 4, we show six successive frames from the simulation. They represent the situation for the values of time 0, 2, 3, 5, 6, and 12 seconds, respectively.

We demonstrate the effect of the constraint stabilization parameter γ, by running the problem for a series of values of $\gamma \in \{0, 0.25, 0.5, 0.75, 1\}$ and $h \in \{0.1, 0.05, 0.02, 0.01\}$. The results are shown in Figure 5, where we clearly see that as the stepsizes increase, the infeasibility grows.

In Figure 6 we fixed $\gamma = 1$ and showed that, as $h \in \{0.1, 0.02, 0.01, 0.002, 0.001\}$, in the limit as the stepsize approaches zero, the behavior of the infeasibility is proportional to the square of the stepsize, which validates Theorem 10.

5.2. Problem: Pyramid1

Despite its name, the Pyramid1 problem is two dimensional and involves a single triangle with nine rectangular bodies arranged in a row. The triangle makes contact with one rectangle, which causes a chain reaction similar to dominoes falling.

We ran the simulation for 10 seconds. At the end of the simulation, the bodies were all at rest.

In Figure 7, we show six successive frames from the simulation. They represent the situation for the values of time 0, 1, 2, 3, 4, and 10 seconds, respectively. The quadratic nature of the constraint stabilization is again demonstrated in Figure 8, when we again fixed $\gamma = 1$ and observed that, as $h \in \{0.1, 0.02, 0.01, 0.002, 0.001\}$, the behavior of the infeasibility is proportional to the square of the stepsize in the limit, again validating Theorem 10.

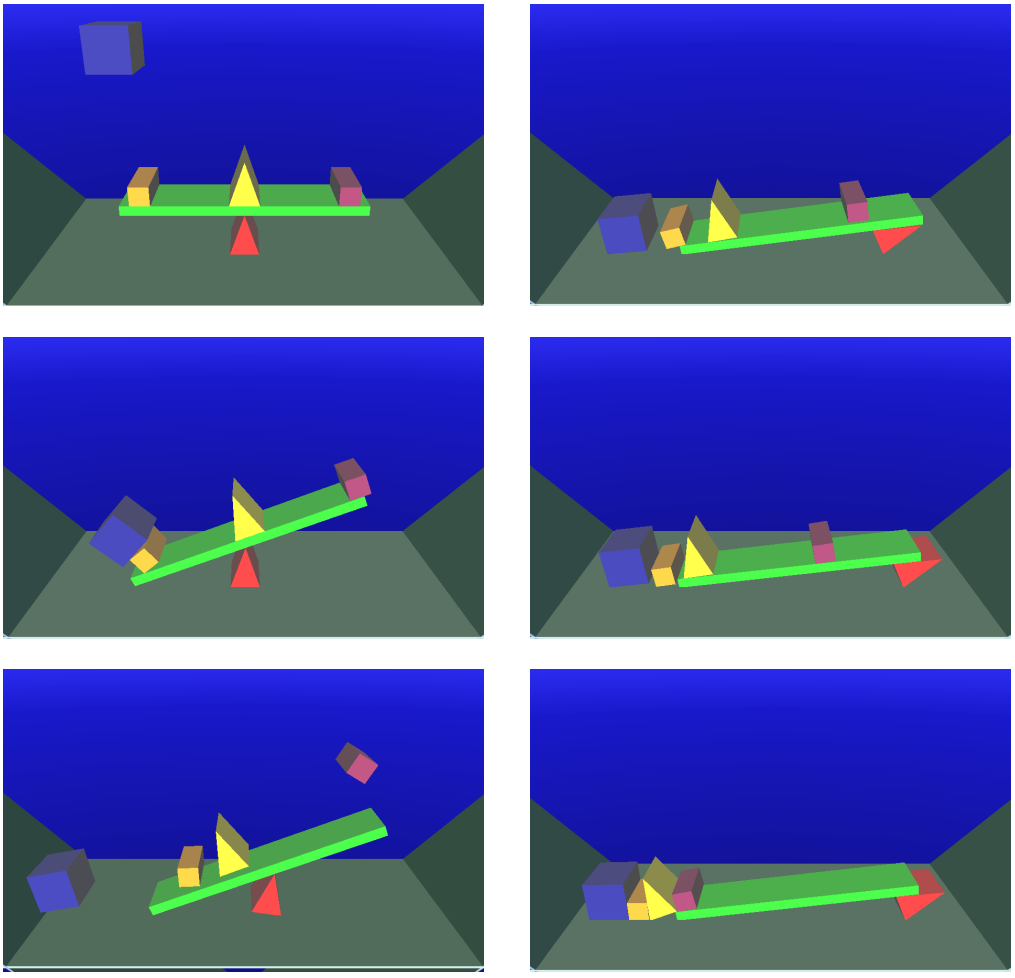

Figure 4: Six successive frames from Balance2

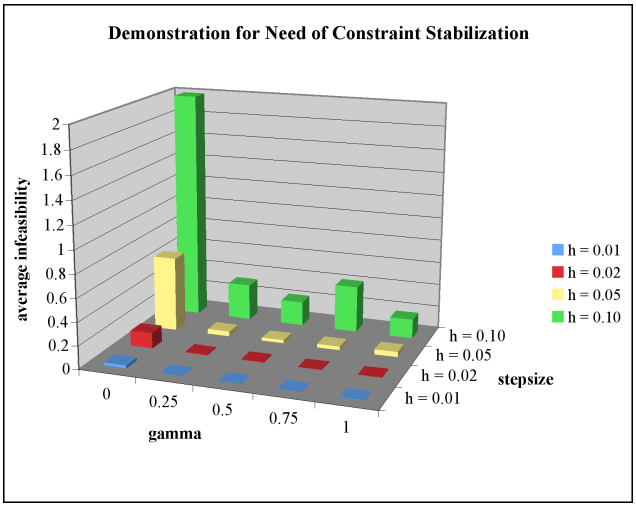

Figure 5: Problem Balance2: effect of constraint stabilization constant γ on infeasibility

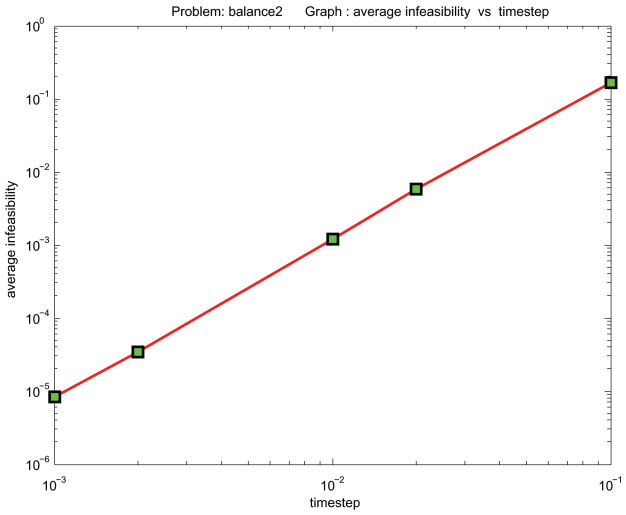

Figure 6: Problem Balance2: infeasibility

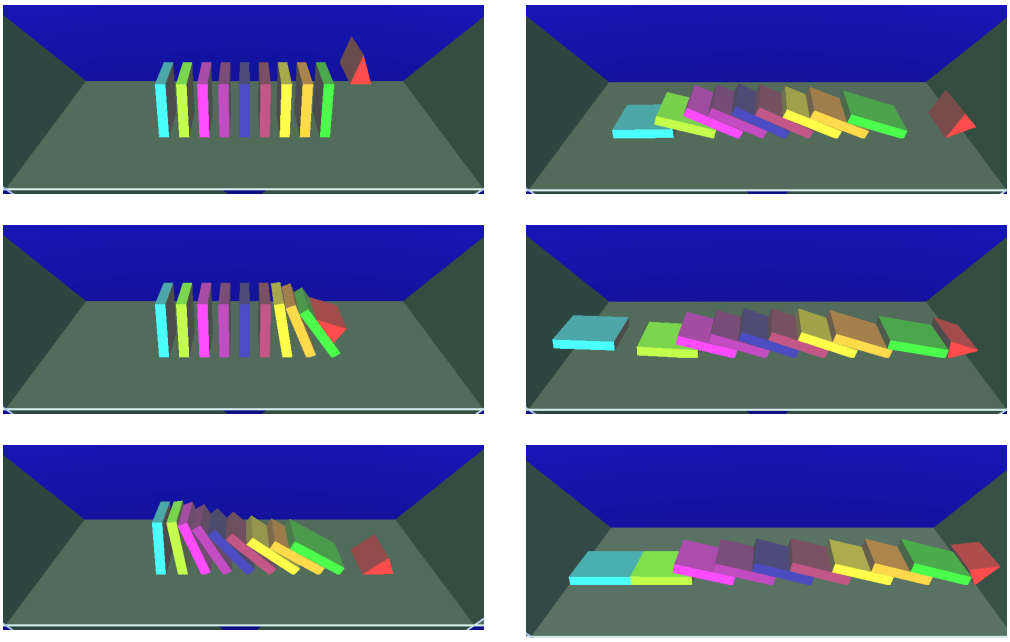

Figure 7: Six successive frames from Pyramid1

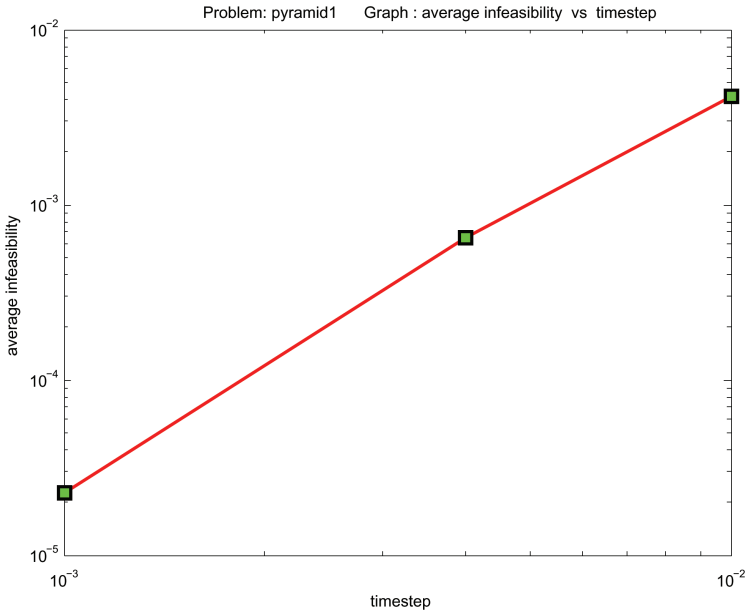

Figure 8: Problem Pyramid1: Infeasibility

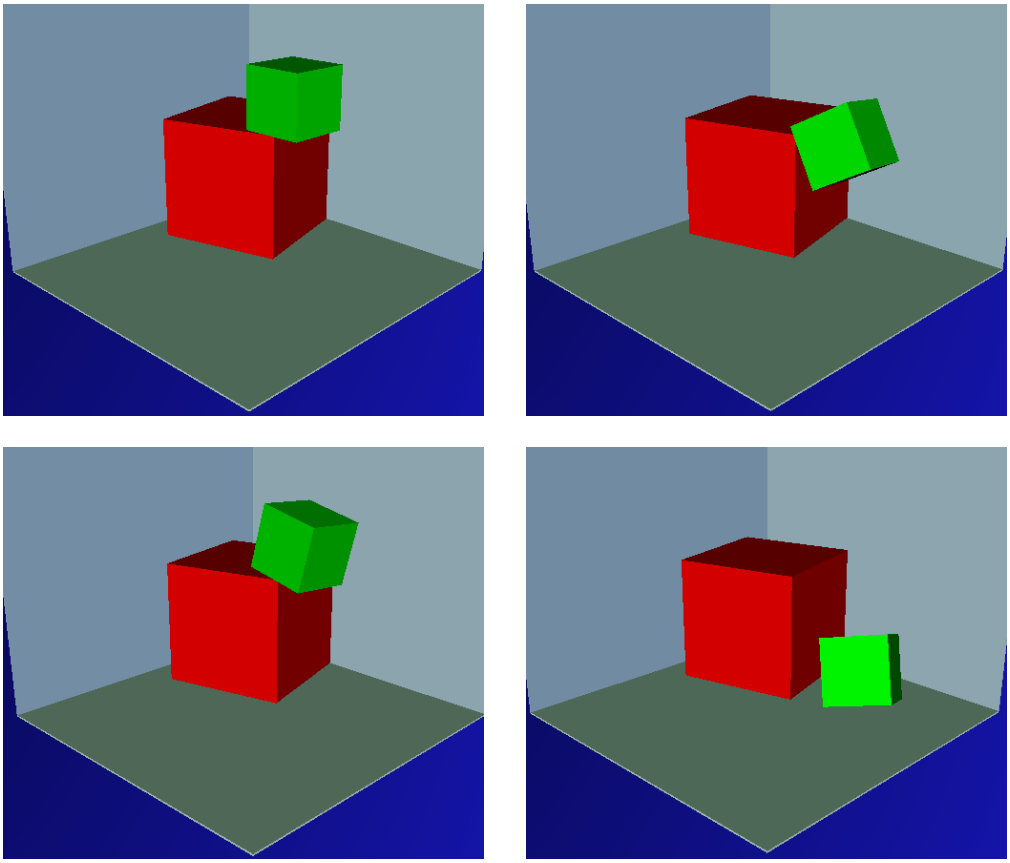

Figure 9: Four successive frames from Dice3

5.3. Problem: Dice3

Our approach applies equally well to a three dimensional problem. The problem we present here is a simple three-dimensional problem involving two cubes, one on top of the other. Gravity causes the cube on top to fall over the edge of the bottom cube.

We ran the simulation for 3 seconds. At the end of the simulation, both of the bodies were on the floor, but the one that fell was not quite at rest. In Figure 9, we show four successive frames from the simulation. They represent the situation for the values of time 0, 1, 2, and 3 seconds, respectively.

We once again noticed the quadratic nature of the constraint stabilization for this three dimensional problem, again seen in Figure 10 when we fixed $\gamma = 1$ and observed that, as $h \in \{0.1, 0.05, 0.01, 0.005\}$, the behavior of the infeasibility is proportional to the square of the stepsize in the limit, again validating Theorem 10 for a 3D case.

5.4. Numerical Summary

We have demonstrated that the ratio metric introduced in this paper is usable for time-stepping RMBD simulation. In addition, Theorem 10 was validated by demonstrating that the

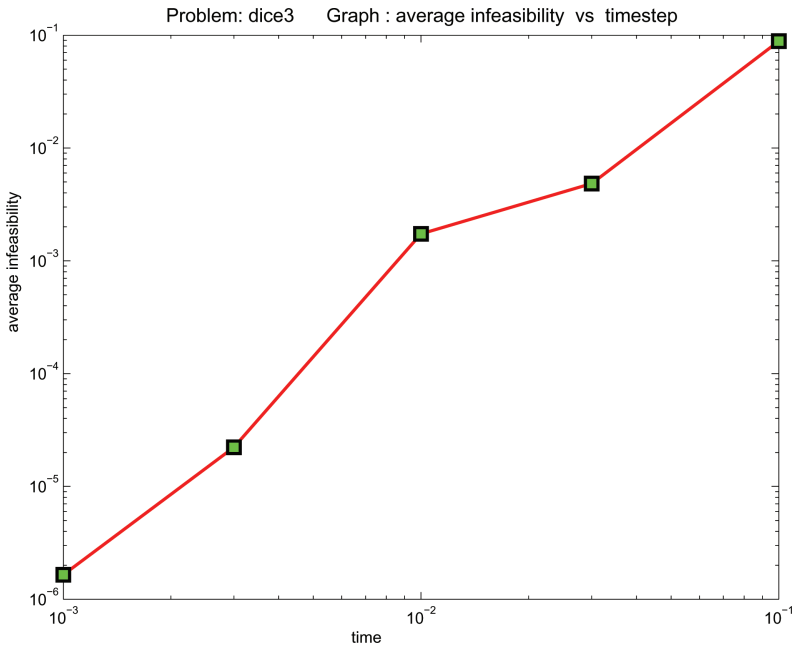

Figure 10: Problem dice3: Infeasibility

infeasibility, as measured by our metric, decreases at least quadratically with the size of the time step. Moreover, the metric equivalence theorem, Theorem 2, *guarantees that the Minkowski penetration depth will decrease with the same asymptotic rate*. Of course, nothing prevents us from using our metric in penalty methods as well; but our demonstration shows that the more complex time-stepping methods as defined in Section 4, work as well.

5.5. Simulations

In this section, we present the video simulations produced by the examples. The goal was to have all motion be realistic and obeying the laws of physics. A simulation of the first example can be seen in Figure 11, which is a QuickTime movie.

The second example was created to display a domino effect, again with realistic results. We have another QuckTime movie in Figure 12, which is our visualization of the simulation.

Our final example was the true three-dimensional problem called dice3. The QuckTime movie Figure 13 is our simulation for this example.

6. Conclusions and Future Research

We have described an $O(m + n)$ penetration depth measure, a new method of determining when two convex polyhedra intersect and measuring the amount of penetration, when it exists. This new method, which defines a signed distance function, has a better theoretical computational complexity than do existing methods for measuring penetration depth. Moreover, it is metrically equivalent to the Minkowski penetration depth, the gold standard for penetration

(QuickTime movie for balance2)

Figure 11: balance2 movie: `http://www.pitt.edu/~gdhart/balance2.mov`

(QuickTime movie for pyramid1)

Figure 12: pyramid1 movie: `http://www.pitt.edu/~gdhart/pyramid1.mov`

depth calculations. After we analyzed differentiation properties of this new measure and described computation of normal vectors at contact, we explained how to implement it in a time-stepping scheme. We demonstrated by several examples that this metric is indeed usable with time-stepping schemes.

(QuickTime movie for dice3)

Figure 13: dice3 movie: `http://www.pitt.edu/~gdhart/dice3.mov`

While the theoretical complexity of our metric is attractive, an important issue is whether this truly results in faster computations. Like most issues having to do with theoretical complexity, decades of investigating various techniques makes a proof difficult in practice. Nevertheless, we plan in the near future to investigate collisions between polyhedra with very large number of faces in order to demonstrate the situation where this algorithm can practically supersede existing approaches. Our ability to characterize the generalized gradient of the metric has resulted in an approach that can work with time-stepping schemes with fixed time step. The lack of smoothness of the gap function has prevented the formal definition of such algorithms in past work. To our knowledge, this is the first time an approach that can work even in principle was proposed. Another interesting area of future investigation is the case of piecewise smooth bodies that are not necessarily polyhedral.

Acknowledgments

Mihai Anitescu was supported by the Office of Advanced Scientific Computing Research, Office of Science, U.S. Dept. of Energy, under Contract DE-AC02-06CH11357.

References

[1] P.K. Agarwal, L.J. Guibas, S. Har-Peled, A. Rabinovitch, M. Sharir, Penetration depth of two convex polytopes in 3d, Nordic Journal in Computing 7 (2000) 227–240.

[2] M. Anitescu, Optimization-based simulation of nonsmooth rigid multibody dynamics, Mathematical Programming 105 (2006) 113–143.

[3] M. Anitescu, J.F. Cremer, F.A. Potra, Formulating 3d contact dynamics problems, Mechanics of Structures and Machines 24 (1996) 405–437.

[4] M. Anitescu, G.D. Hart, Solving nonconvex problems of multibody dynamics with joints, contact, and small friction by successive convex relaxation, Mechanics Based Design of Structures and Machines 31 (2003) 335–356.

[5] M. Anitescu, G.D. Hart, A constraint-stabilized time-stepping approach for rigid multibody dynamics with joints, contact and friction, International Journal for Numerical Methods in Engineering 60 (2004) 2335–2371.
[6] M. Anitescu, G.D. Hart, A fixed-point iteration approach for multibody dynamics with contact and small friction, Mathematical Programming 101 (2004) 3–32.
[7] M. Anitescu, A. Miller, G.D. Hart, Constraint stabilization for time-stepping approaches for rigid multibody dynamics with joints, contact and friction, in: Proceedings of the 2003 ASME International Design Engineering Technical Conferences, American Society for Mechanical Engineering, Chicago, Illinois, 2003. ANL/MCS-P1023-0403.
[8] M. Anitescu, F.A. Potra, Formulating dynamic multi-rigid-body contact problems with friction as solvable linear complementarity problems, Nonlinear Dynamics 14 (1997) 231–247.
[9] M. Anitescu, F.A. Potra, On integrating stiff rigid multibody dynamics with contact and friction, in: Contact Mechanics. Proceedings of the 3rd Contact Mechanics International Symposium, Praia de Consola cão, Peniche, Portugal, June 17-21, 2001, Kluwer Academic Publishers, Dordrecht, Netherlands, 2002.
[10] M. Anitescu, F.A. Potra, D. Stewart, Time-stepping for three-dimensional rigid-body dynamics, Computer Methods in Applied Mechanics and Engineering 177 (1999) 183–197.
[11] Y. Baillot, J.P. Rolland, D.L. Wright, Automatic modeling of knee-joint motion for the virtual reality dynamic anatomy (vrda) tool", Presence: Teleoperators and Virtual Environments (MIT Press) 9 (3) (2000) 223 – 235.
[12] D. Baraff, Issues in computing contact forces for non-penetrating rigid bodies, Algorithmica 10 (1993) 292–352.
[13] F.H. Clarke, Optimization and Nonsmooth Analysis, volume 5 of *SIAM Classics in Applied Mathematics*, SIAM, Philadelphia, 1990.
[14] J.F. Cremer, D.E. Stewart, The architecture of newton, a general purpose dynamics simulator, in: Proceedings of the IEEE International Conference in Robotics and Automation, IEEE, 2003, pp. 1806–1811.
[15] B.R. Donald, D.K. Pai, On the motion of compliantly connected rigid bodies in contact: a system for analyzing designs for assembly, in: Proceedings of the Conf. on Robotics and Automation, IEEE, 1990, pp. 1756–1762.
[16] C. Glocker, F. Pfeiffer, An lcp-approach for multibody systems with planar friction, in: Proceedings of the CMIS 92 Contact Mechanics Int. Symposium, Lausanne, Switzerland, pp. 13 – 30.
[17] C. Glocker, F. Pfeiffer, Multiple impacts with friction in rigid multi-body systems, Nonlinear Dynamics 7 (1995) 471–497.
[18] G.D. Hart, A constraint-stabilized time-stepping approach for piecewise smooth multibody dynamics, Ph.D. thesis, University of Pittsburgh, Pittsburgh, PA 15260, 2007.
[19] G.D. Hart, M. Anitescu, A hard-constraint time-stepping approach for rigid multibody dynamics with joints, contact, and friction, in: J. Meza, B. York (Eds.), Proceedings of the Richard Tapia Celebration of Diversity in Computing Conference 2003, ACM Press, New York, NY, USA, 2003, pp. 34–41.
[20] E.J. Haug, Computer Aided Kinematics and Dynamics of Mechanical Systems. Vol. 1: Basic Methods, Allyn & Bacon, Inc., Needham Heights, MA, USA, 1989.
[21] L. Hodges, P.L. Anderson, G.C. Burdea, H.G. Hoffman, B.O. Rothbaum, Treating psychological and physical disorders with VR, IEEE Computer Graphics and Applications (2001) 25–33.
[22] Y. Kim, M. Otaduy, M. Lin, D. Manocha, Fast penetration depth computation for physically-based animation, in: Proceedings of the 2002 ACM SIGGRAPH/Eurographics Symposium on Computer Animation, ACM, pp. 23–31.
[23] Y.J. Kim, M.C. Lin, D. Manocha, Deep: Dual-space expansion for estimating penetration depth between convex polytopes, in: Proceedings of the 2002 International Conference on Robotics and Automation, volume 1, Institute for Electrical and Electronics Engineering, 2002, pp. 921–926.
[24] Y.J. Kim, M.A. Otaduy, M.C. Lin, D. Manocha, Fast penetration depth computation for physically-based animation, in: J. Hodgins, M. van de Panne (Eds.), Proceedings of the 2002 ACM Siggraph/Eurograph Symposium on Computer Animation, Association for Computing Machinery, San Antonio, Texas, 2002, pp. 21 – 33.
[25] N. Megiddo, Linear-time algorithms for linear programming in r^3 and related problems, SIAM Journal on Computing 12 (1983) 759–776.
[26] A. Miller, H.I. Christensen, Implementation of multi-rigid-body dynamics within a robotic grasping simulator, in: IEEE International Conference on Robotics and Automation, pp. 2262–2268.
[27] B. Mirtich, Impulse-based Dynamic Simulation of Rigid Body Systems, Ph.D. thesis, University of California, Berkeley, 1996.
[28] T.B. Moeslund, E. Granum, A survey of computer vision-based human motion capture, Computer Vision and Image Understanding 81 (2001) 231–268.
[29] J. Moreau, Numerical aspects of the sweeping process, Computer Methods in Applied Mechanics and Engineering 177 (1999) 329–349.
[30] B.O. Rothbaum, L. Hodges, P.L. Anderson, L. Price, S. Smith, Twelve-month follow-up of virtual reality and standard exposure therapies for the fear of flying, Journal of Consulting and Clinical Psychology 70(2) (2002) 428–432.
[31] B.O. Rothbaum, L. Hodges, D. Ready, K. Graap, R.D. Alarcon, Virtual reality exposure therapy for vietnam veter-

ans with posttraumatic stress disorder, Journal of Clinical Psychiatry 62(8) (2001) 617–622.
[32] W.J. Shiu, F.V. Donzé, S.A. Magnier, Numerical study of rockfalls on covered galleries by the discrete element method, Electronic Journal of Geotechnical Engineering 11 Bundle D (2006).
[33] P. Song, P. Kraus, V. Kumar, P. Dupont, Analysis of rigid-body dynamic models for simulation of systems with frictional contacts, Journal of Applied Mechanics 68 (2001) 118–128.
[34] D.E. Stewart, Rigid-body dynamics with friction and impact, SIAM Review 42 (2000) 3–39.
[35] D.E. Stewart, J.C. Trinkle, An implicit time-stepping scheme for rigid-body dynamics with inelastic collisions and coulomb friction, International Journal for Numerical Methods in Engineering 39 (1996) 2673–2691.
[36] J. Trinkle, J.S. Pang, S. Sudarsky, G. Lo, On dynamic multi-rigid-body contact problems with coulomb friction, Zeithschrift fur Angewandte Mathematik und Mechanik 77 (1997) 267–279.
[37] T. Weiner, Pentagon has sights on robot soldiers, 2005. New York Times News Service, appearing in The San Diego Union-Tribune, available online at *http://www.signonsandiego.com/uniontrib/20050216/news_1n16robot.html* .
[38] ZZZ1, Stanford team wins robot race, online, 2005. Associated Press, available online from MSNBC.com at *http://www.msnbc.msn.com/id/9621761/*.